J Supercond Nov Magn (2015) 28:3557–3564
DOI 10.1007/s10948-015-3192-5

ORIGINAL PAPER

Enhanced Saturation Magnetization in Cobalt Doped Ni-Zn Ferrite Nanoparticles

Rajinder Kumar[1] · Hitanshu Kumar[1] · Manoj Kumar[2] · Ragini Raj Singh[1] · P. B. Barman[1]

Received: 15 May 2015 / Accepted: 23 July 2015 / Published online: 14 August 2015

Abstract The Co substitution in Ni-Zn ferrites with respect to their structural and magnetic properties has been investigated in favor to select a material for future electromagnetic interference (EMI) shielding application purpose. $Ni_{0.6-x}Zn_{0.4}Co_xFe_2O_4$ ($x = 0, 0.03, 0.09, 0.27$) nanoparticles were synthesized using a sol-gel method and annealed at 700 °C. The prepared $Ni_{0.6-x}Zn_{0.4}Co_xFe_2O_4$ samples were characterized for their structural, stoichiometric, and magnetic properties. X-ray diffraction patterns reveal the formation of single-phase spinel cubic structure formed at $x = 0.27$. The influence of Co doping on structural properties of Ni-Zn ferrite was examined with X-ray diffraction and field emission scanning electron microscopy. The stoichiometry of prepared samples has also been examined by energy-dispersive X-ray spectroscopy. The magnetic behavior was studied using a vibrating sample magnetometer at room temperature. The variations in values of saturation magnetization were explained on the basis of spin canting effect imparted by hematite (α-Fe_2O_3) phase with spinel phase. $Ni_{0.6-x}Zn_{0.4}Co_xFe_2O_4$ with $x = 0.27$ possesses best saturation magnetization and can be useful in EMI shielding material.

✉ Ragini Raj Singh
raginirajsingh@gmail.com

[1] Department of Physics and Materials Science, Jaypee University of Information Technology, Waknaghat, Solan 173234, Himachal Pradesh, India

[2] Department of Physics and Materials Science, Jaypee Institute of Information Technology, A-10, Sector-62, Noida 201307, Uttar Pradesh, India

Keywords Ferrimagnetic · Solgel method · Structural properties · Magnetic properties

1 Introduction

The last decade has been marked for the spinel ferrites as these materials become promising candidates for emerging research by virtue of their good magnetic properties and high resistivity over a wide range of frequencies (few hundred Hz to several GHz). Spinel ferrites are technologically very important materials because of their magnetic, electrical, and optical properties, having a general formula of MFe_2O_4 (where M is divalent metal cations such as Fe^{2+}, Co^{2+}, Ni^{2+}, Zn^{2+}, etc.). These ferrites have been widely used in electronic and magnetic devices because of their unique properties like high magnetic permeability, low magnetic losses, high thermal stability, high electrical resistivity, electrolytic activity, and resistance to corrosion [1, 2]. The chemical, structural, electrical, and magnetic properties of spinel ferrites are strongly influenced by their compositions, synthesis methods, and cation substitutions [3]. Nowadays, soft ferrimagnetic Ni-Zn ferrites are a subject of intense research because they possess high resistivity, moderate saturation magnetization, low coercivity, high Curie temperature, good mechanical hardness, and chemical stability [4]. Owing to their excellent properties, Ni-Zn ferrites are promising magnetic materials used in many applications such as antenna rods, recording heads, loading coils, core materials for power applications, microwave devices, etc. [5–8].

The magnetic properties of Ni-Zn ferrites can be enhanced by doping of various metals such as chromium, copper, manganese, cobalt, zinc, etc. [9]. Doped Ni-Zn ferrites possess high resistivity and high permeability and can

be used in radio-frequency (RF) electronic device applications [10]. Codoped Ni-Zn ferrites are a very much approved material in electromagnetic interference (EMI) shielding applications. B. P. Rao et al. [11] reported the Co-dependent magnetic behavior of $Ni_{0.35}Zn_{0.65-x}Co_xFe_2O_4$ ($x = 0$ to 0.25) synthesized using a conventional ceramic technique. S. R. Shannigrahi et al. [12] described the EMI shielding nature of $(Ni_xR_{1-x})_{0.5}Zn_{0.5}Fe_2O_4$ composite thin film prepared by microwave sintering and melt blending approach (R = Mn, Co, Cu; $x = 0, 0.5$). It has been found that, among the different dopants, Codoped ferrite shows the best saturation magnetization and high EMI shielding effectiveness value. X. Shen et al. [13] also studied the microwave absorbing properties of $(Ni_xZn_{1-x})Co_yFe_{2-y}O_4$ ($x = 0.0$, 0.4, 0.5, 0.6; $y = 0.0$, 0.01) synthesized using a hydrothermal route and showed an increased saturation magnetization as a function of Co doping. J. S. Ghodake et al. [14] have reported the permeability and magnetic behavior of Co-substituted Ni-Zn ferrites processed using an oxalate precursor method. S. L. Pereira et al. [15] investigated the modified magnetic behavior of Cosubstituted Ni-Zn ferrite synthesized using a hydrothermal process. L.-Z. Li et al. [16] studied the influence of Cu and Co substitution on the properties of Ni-Zn ferrite thin films synthesized using a solgel method. On the basis of the above discussion, here, this work is intended to study the magnetic properties of Codoped Ni-Zn ferrite. The soft magnetic materials are used as EMI shielding materials, having a high value of saturation magnetization and a low value of coercivity. Consequently, Co has been introduced in Ni-Zn ferrite to enhance the saturation magnetization. There are very few reports available on Codoped Ni-Zn ferrite nanoparticles for EMI shielding application. In the present paper, distinctive composition of $Ni_{0.6-x}Zn_{0.4}Co_xFe_2O_4$ ($x = 0, 0.03, 0.09, 0.27$) has been reported. Ni-Zn ferrite has been doped with Co and processed using a solgel method because of exclusive advantages like low processing temperature, homogeneous reaction distribution, excellent composition control, costeffectiveness, and better results over other complex methods. The effect of cobalt doping on structure, morphology, stoichiometry, and magnetic properties has been studied on the basis of Co ion distribution and spin canting effect by X-ray diffraction (XRD), field emission scanning electron microscopy (FESEM), energy-dispersive X-ray spectroscopy (EDX), and vibrating sample magnetometer (VSM), respectively.

2 Experimental Details

2.1 Synthesis of Ni-Zn Ferrite and Co-Doped Ni-Zn Ferrite Nanoparticles

The ferrite nanoparticles have been synthesized using a solgel method. The chemicals nickel nitrate hexahydrate ($Ni(NO_3)_2{\cdot}6H_2O$), zinc nitrate hexahydrate ($Zn(NO_3)_2 \cdot 6H_2O$), cobalt nitrate hexahydrate ($Co(NO_3)_2 \cdot 6H_2O$), ferric nitrate nonahydrate ($Fe(NO_3)_3 \cdot 9H_2O$), and citric acid monohydrate ($C_6H_8O_7$) were used as raw materials to prepare $Ni_{0.6-x}Zn_{0.4}Co_xFe_2O_4$ ($x = 0, 0.03, 0.09, 0.27$) nanoparticles. The appropriate amounts of nitrates were dissolved in distilled water under magnetic stirring for 30 min, and then citric acid monohydrate was dissolved in it with a nitrate-to-citric acid molar ratio of 1:3. Ammonia solution

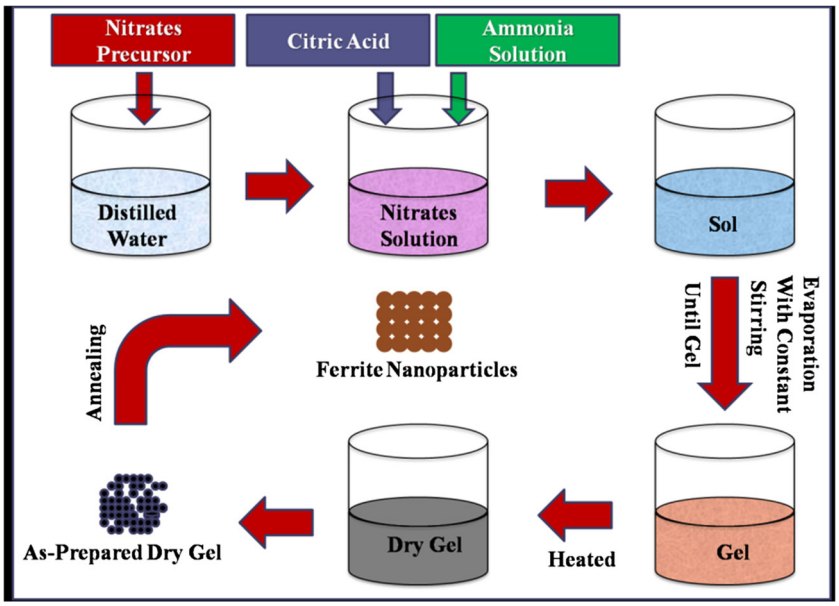

Fig. 1 Schematic diagram of sol-gel method to synthesize $Ni_{0.6-x}Zn_{0.4}Co_xFe_2O_4$

was added into the solution to an adjusted pH level of 7, kept at 75 °C, and stirred continuously until the solution changed into gel. The gel was dried at 110 °C for 24 h and annealed at 700 °C for 5 h. Finally, desired ferrite nanoparticles have been obtained. An schematic diagram of sol-gel method is shown in Fig. 1.

2.2 Characterization

Prepared $Ni_{0.6-x}Zn_{0.4}Co_xFe_2O_4$ (NZCF) ($x = 0$, 0.03, 0.09, 0.27) samples were characterized by Shimadzu-6000 XRD using Cu-Kα ($\lambda = 1.546\mathring{A}$) radiation for phase identification, measurement of crystallite size, and other structural parameters. Morphology and elemental analysis of the prepared samples were observed by Carl Zeiss Modal No-Ultra Plus-55 FESEM and Oxford Instruments EDX, respectively. The effect of Co doping on the magnetic properties of Ni-Zn ferrite has been examined by PAR-155 VSM in a magnetic field range from −10 to +10 KOe.

3 Results and Discussions

3.1 Structural Characterization

Structural analysis of the $Ni_{0.6-x}Zn_{0.4}Co_xFe_2O_4$ ($x = 0$, 0.03, 0.09, 0.27) samples has been performed using the powder XRD patterns and is presented in Fig. 2. The XRD peaks (111), (022), (113), (222), (004), (224), (333), and (044) indicate that the prepared sample at $x = 0.27$ has a single-phase spinel cubic structure. The other prepared samples at $x = 0$, 0.03, and 0.09 have partial formation of secondary hematite phase with spinel-phase cubic structure. In the reported literature, it has been found that the Ni-Zn ferrite nanoparticles prepared using a sol-gel method and annealed below 700 °C have single-phase spinel structure [17, 18]. The diffraction peaks have good agreement with standard JCPDS card nos. 52-0277 and 89-0599 corresponding to spinel Ni-Zn ferrite and secondary hematite phase, respectively. The peak intensity of secondary hematite phase is in the order $I_{x=0.03} > I_{x=0.09} > I_{x=0}$ and it also found that secondary phase diminished at high concentration of cobalt doping. The average crystallite size of all prepared samples has been calculated from full width at half maximum (FWHM) of most prominent peak (113) of XRD patterns using Scherer's (1) [19].

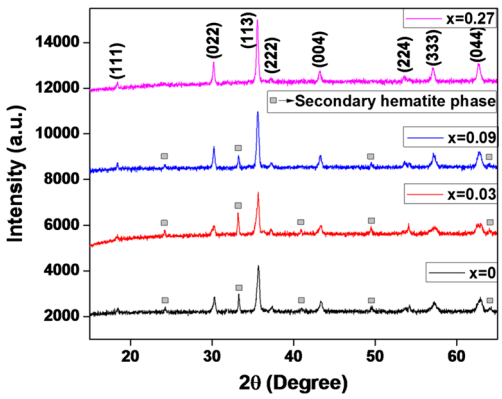

Fig. 2 XRD spectra of $Ni_{0.6-x}Zn_{0.4}Co_xFe_2O_4$ ($x = 0$, 0.03, 0.09, 0.27)

$$D = 0.9\lambda/\beta\cos\theta \tag{1}$$

where D is the average crystallite size, β is the FWHM of the peak intensity measured in radians, $\lambda = 1.54$ Å is the wavelength of X-ray, and θ is Bragg's angle. It is found that crystallite size (D) increases with cobalt doping from 25 to 31 nm. This might be due to the replacement of Ni^{2+} (ionic radii = 0.69 Å) ions by larger Co^{2+} (ionic radii = 0.745 Å) ions in octahedral sites, resulting to size enlargement of unit cells. The crystallite size (D) obtained at $x = 0.03$ (28 nm) and $x = 0.09$ (29 nm) is nearly the same. Also, other calculated structural parameters at $x = 0.03$ and 0.09 possess approximately the same values by virtue of this small dopant variation. Hence, the calculated crystallite size (D) and other structural parameters at $x = 0.09$ are not listed in the table.

The effect of Co doping on structural parameters includes d spacing (d) [20] and lattice constant (a) [21] that have been calculated and presented in Table 1, using the following relations (2 and 3):

$$2d\sin\theta = n\lambda \tag{2}$$

$$a = d \times \sqrt{h^2 + k^2 + l^2} \tag{3}$$

It has been noticed that the d spacing (d) as well as the lattice constant (a) decreased at $x = 0.03$ and then increased

Table 1 Crystallite size (D), d spacing (d), and lattice constant (a) calculated from the prominent peak (113) of XRD; crystallite size (W-H D); and strain (W-H ε) calculated from Williamson-Hall plots at $x = 0$, 0.03, and 0.27

x (Co doping)	D (nm)	d (Å)	a (Å)	W-H	
				D (nm)	ε
0.00	25	2.5209	8.3608	30	0.0170
0.03	28	2.5195	8.3563	33	0.0176
0.27	31	2.5209	8.3608	32	0.0111

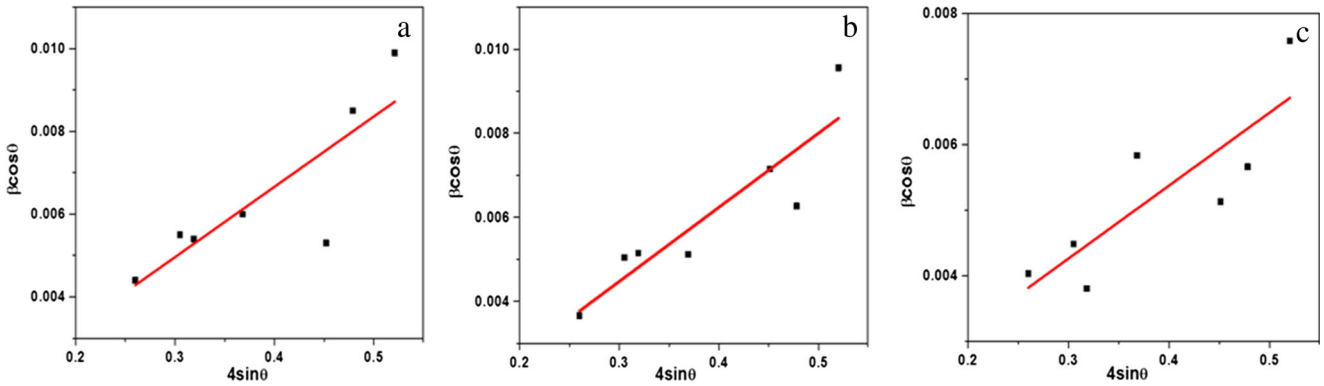

Fig. 3 W-H plots of $Ni_{0.6-x}Zn_{0.4}Co_xFe_2O_4$ at **a** $x = 0$, **b** $x = 0.03$ and **c** $x = 0.27$

at $x = 0.27$ value of Co doping. The slight decrease in lattice constant (a) at $x = 0.03$ value of Co doping is attributed to lattice shrinkage caused by segregation of Co^{2+} ions at grain boundaries and, possibly, by high secondary phase effect. The crystallite size (W-H D) and strain (W-H ε) estimated from Williamson-Hall (W-H) method is inscribed in Table 1. The width of individual reflections in the W-H method has been expressed by Eq. 4 [22].

$$\beta \cos\theta = k\lambda/D + 4\varepsilon \sin\theta \tag{4}$$

where β is the FWHM of peaks, D is the crystallite size, λ is the wavelength of Cu-Kα radiation, and ε is the strain. Figure 3a–c shows the W-H plots for $x = 0.0$, 0.03, and 0.27, respectively. The obtained values of crystallite size (W-H D) from W-H plots are approximately equivalent to those calculated using Scherer's formula. The positive slope of the linear fit in W-H plots shows a tensile strain present in all prepared samples [22]. The tensile strain firstly increased at $x = 0.03$ and then decreased at $x = 0.27$ value of Co doping. The increased tensile strain at $x = 0.03$ is attributed to lattice distortion caused by high secondary hematite phase effect. Finally, it is concluded that the strain present in the crystal structure is proportional to the concentration of the secondary hematite phase with primary phase.

3.2 FESEM-EDX Characterizations

The prepared samples were further characterized by FESEM for morphological study. Figure 4 shows the FESEM micrographs of $Ni_{0.6-x}Zn_{0.4}Co_xFe_2O_4$ ($x = 0$, 0.03, 0.27). It is observed that the morphology of prepared samples is very similar to each other. The crystallinity increased with Co^{2+} doping has been marked, and the particle sizes lie in nanometer range, having fairly narrow size distribution with some agglomeration of particles.

The stoichiometry study of prepared samples has been performed by EDX. The EDX spectra of $Ni_{0.6-x}Zn_{0.4}Co_xFe_2O_4$ ($x = 0$, 0.03, 0.27) are being presented in Fig. 5a–c. The results revealed that the prepared samples other than $x = 0.27$ composition are in off-stoichiometry. At $x = 0.27$, all the elements are found in expected composition. The obtained ratio of O:Fe:Ni:Co:Zn is 4:2:0.33:0.27:0.4 at $x = 0.27$. On the basis of these findings, it has been concluded that the sample prepared at $x = 0.27$ attains good stoichiometry.

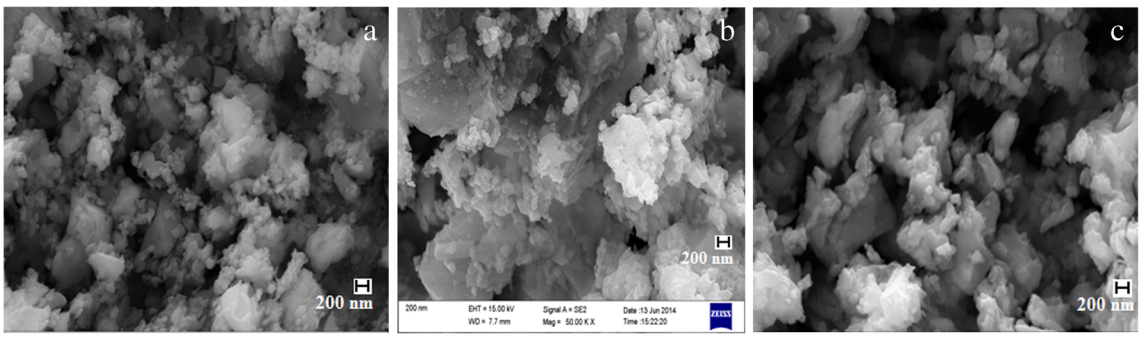

Fig. 4 FESEM micrographs of $Ni_{0.6-x}Zn_{0.4}Co_xFe_2O_4$ at **a** $x = 0$, **b** $x = 0.03$ and **c** $x = 0.27$

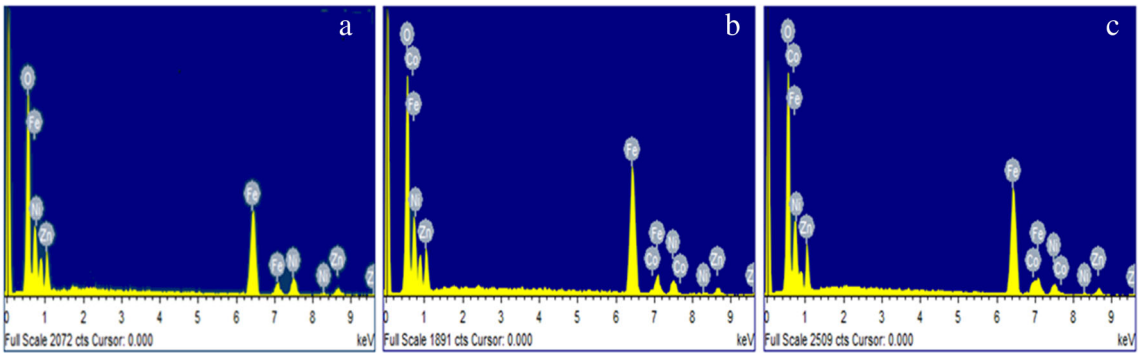

Fig. 5 EDX micrographs of $Ni_{0.6-x}Zn_{0.4}Co_xFe_2O_4$ at **a** $x = 0$, **b** $x = 0.03$ and **c** $x = 0.27$

3.3 Magnetic Characterization

The magnetic properties of $Ni_{0.6-x}Zn_{0.4}Co_xFe_2O_4$ ($x = 0$, 0.03, 0.09, 0.27) have been studied using a VSM at room temperature and are illustrated in Fig. 6a–d. The obtained values of saturation magnetization (M_s), retentivity (M_r), coercivity (H_c), and squareness ratio (M_r/M_s) from the VSM are listed in Table 2.

The magnetization of ferrite material strongly depends upon the super-exchange interaction between octahedral (B) and tetrahedral (A) site magnetic ions. The net magnetic moment (M) of the lattice is $M = M$ (B) $- M$ (A) where M (B) and M (A) are the magnetic moments of B and A sites, respectively [23]. Ni-Zn ferrite has a mixed spinel structure. The octahedral sites are occupied by Ni^{2+} and Fe^{3+} ions, whereas tetrahedral sites are occupied by Zn^{2+} and Fe^{3+} ions [24]. Co^{2+} ions have tendency to occupy octahedral sites [25]. The standard magnetic moment values of Zn^{2+}, Ni^{2+}, Co^{2+}, and Fe^{3+} ions are 0, 2, 3 and 5 μ_B respectively. The obtained value of saturation magnetization (M_s) is 35.61, 29.58, 30.57 and 59.75 emu/g at $x = 0$, 0.03, 0.09 and 0.27 respectively. The observed

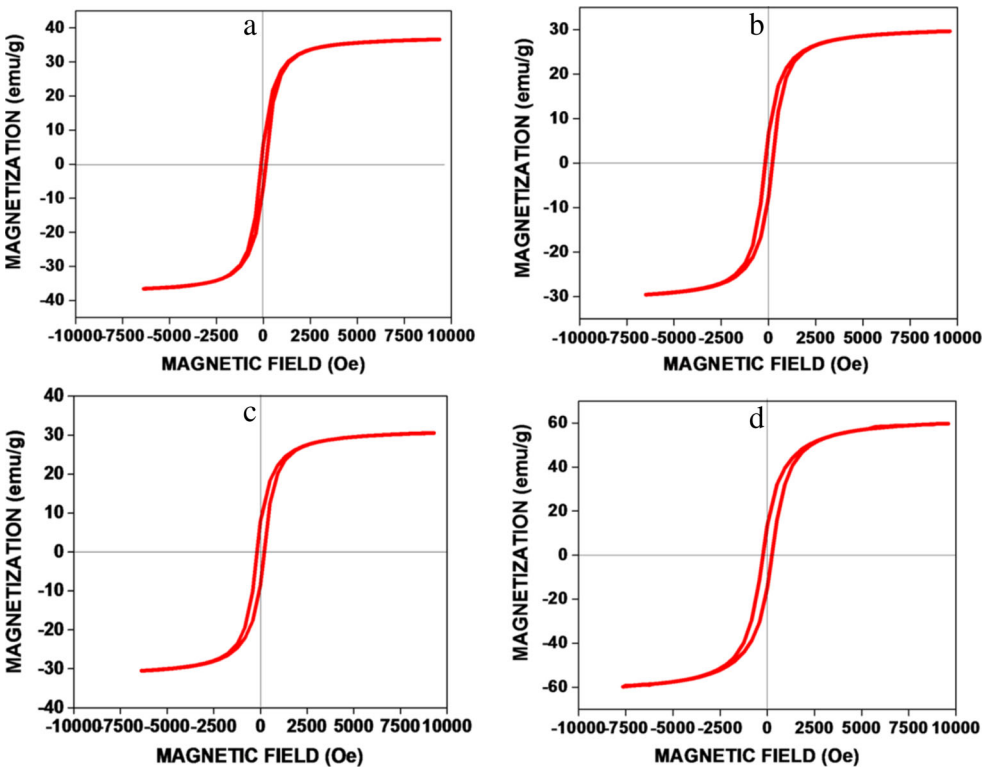

Fig. 6 Hysteresis loops of $Ni_{0.6-x}Zn_{0.4}Co_xFe_2O_4$ at **a** $x = 0$, **b** $x = 0.03$, **c** $x = 0.09$ and **d** $x = 0.27$ at room temperature (300 K)

Table 2 Saturation magnetization (M_s), retentivity (M_r), coercivity (H_c), and squareness ratio (M_r/M_s) measured using a VSM

x (Co doping)	M_s (emu/g)	M_r (emu/g)	H_c (Oe)	M_r/M_s
0.00	35.61	06.24	126.28	0.1752
0.03	29.58	07.15	188.00	0.2417
0.09	30.57	08.98	193.11	0.2937
0.27	59.75	14.26	236.46	0.2386

variation in saturation magnetization (M_s) is explained on the basis of Co doping and secondary hematite phase. The effect of secondary hematite phase on saturation magnetization (M_s) is explained on the basis of spin canting effect (Fig. 7). The low value of saturation magnetization (M_s) at $x = 0.03$ by virtue of anti-ferromagnetic hematite phase is present in large extent with spinel phase. The interaction of anti-ferromagnetic hematite phase with ferromagnetic spinel phase causes the dominant spin canting and decreases the total magnetic moment. This consequently decreases the saturation magnetization (M_s) of the system [26].

The obtained values of saturation magnetization and canting effect at $x = 0.03$ and 0.09 have been found nearly the same because of this much small dopant variation as can be seen in Table 2. Increased saturation magnetization (M_s) at $x = 0.27$ is credited to high magnetic moment of Co^{2+} (3 μ_B) ions. The Co^{2+} (3 μ_B) ions replace the Ni^{2+} (2 μ_B) ions in B sites and increase the B site magnetic moment. These consequently increase the super-exchange interaction and total magnetic moment. Thus, the increase in saturation magnetization (M_s) is observed. The value of coercivity (H_c) has been slightly increased with Co doping because of their high crystalline anisotropy energy. The above results show that all prepared powder samples are magnetically soft in nature and, among them at $x = 0.27$, have highest saturation magnetization value. The best magnetic behavior at $x = 0.27$ indicates that this material can be useful in EMI shielding material. The relation between Co doping, crystallite size (D), saturation magnetization (M_s), coercivity (H_c), secondary phase, and strain (W-H ε) is shown in Fig. 8. It is concluded that crystallite size (D) increases with Co doping because of larger ionic radii of Co^{2+} (0.745 Å) ions as compared to Ni^{2+} (0.69 Å). The value of coercivity (H_c) increases with Co doping. The high crystalline anisotropy energy of Co^{2+} ions slight increases the value of coercivity (H_c) in ferrite. The secondary hematite phase found in the prepared samples first increased at $x = 0.03$ and then decreased with cobalt doping and diminished at $x = 0.27$.

Figure 8 shows that as secondary phase increases in the samples, strain also increases. It means that strain is proportional to the secondary hematite phase. The saturation magnetization (M_s) is also strongly influenced by secondary hematite phase. The secondary hematite phase with spinel phase is greater, resulting to higher spin canting effect which, in turn, reduces the value of saturation magnetization (M_s). The saturation magnetization (M_s) of the ferrite inversely depends on the secondary hematite phase. The behavior of sample at $x = 0.09$ is not included in Fig. 8 because of the findings of nearly the same crystallite size (D) and similar magnetic behavior as observed in the sample at $x = 0.03$.

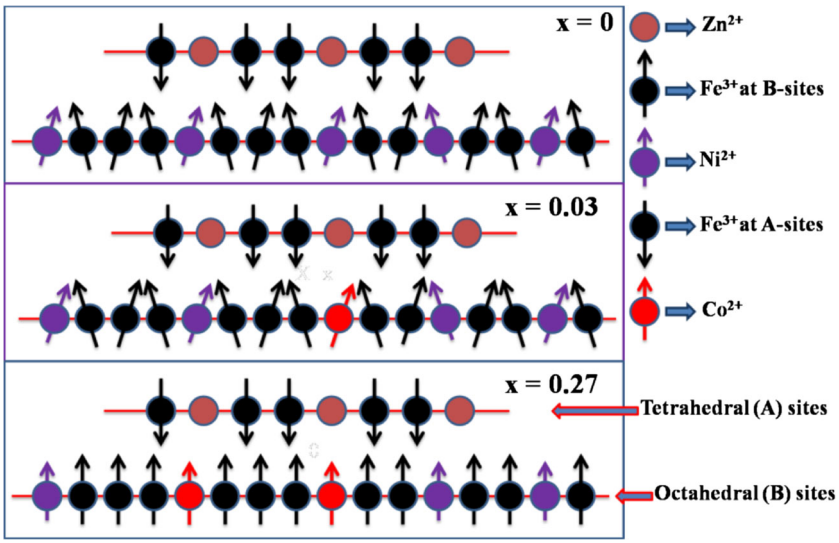

Fig. 7 Spin canting behavior in $Ni_{0.6-x}Zn_{0.4}Co_xFe_2O_4$ systems on Co doping

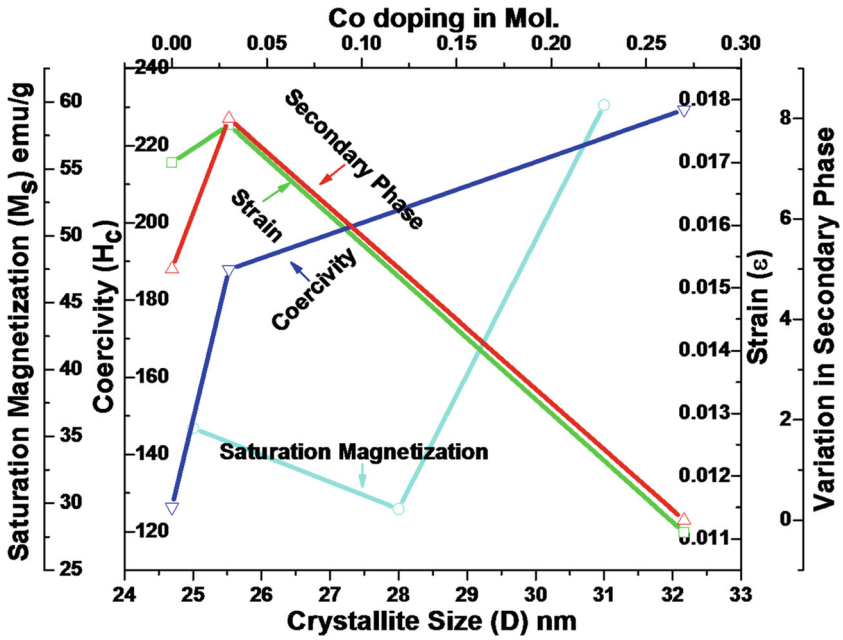

Fig. 8 The relation between Co doping, crystallite size (D), saturation magnetization (M_s), coercivity (H_c), secondary phase, and strain (W-H ε)

4 Conclusion

The present study demonstrated the effect of Co doping on structural and magnetic properties of $Ni_{0.6-x}Zn_{0.4}Co_xFe_2O_4$ ($x = 0, 0.03, 0.09, 0.27$) synthesized using a solgel method. XRD study revealed that samples prepared at $x = 0.27$ have singlephase spinel cubic structure. There is partial formation of secondary hematite phase (α-Fe_2O_3) with spinelphase cubic structure of $Ni_{0.6x}Zn_{0.4}Co_xFe_2O_4$ ($x = 0, 0.03, 0.09$). The crystallite size (D) increases with Co doping because of larger ionic radii of Co^{2+} ions as compared to Ni^{2+} ions. The secondary phase firstly increased with Co doping ($x = 0.03$) and then decreased with Co doping ($x = 0.09$) and diminished at high concentration of Co doping ($x = 0.27$). The strain present in the crystal structure also increases with secondary phase because of lattice distortion produced by secondary phase. The crystallinity of prepared samples increases with Co doping and has been investigated by FESEM. EDX study revealed that all the elements which are present in the sample at $x = 0.27$ are desired and in stoichiometric ratio, but the samples other than this are in off-stoichiometry. The saturation magnetization (M_s) firstly decreases with Co doping and then increases as observed from a VSM study. The reduced value of saturation magnetization (M_s) at $x = 0.03$ is attributed to the dominant spin canting effect caused by prominent secondary phase found in the sample. The values of retentivity (M_r) as well as coercivity (H_c) increased with Co doping due to the anisotropy energy of Co imparted in Ni-Zn ferrite. Similar crystallite size (D) and magnetic behavior observed at $x = 0.03$ and 0.09 because of minute dopant variation. The higher value of saturation magnetization at $x = 0.27$ indicates that this material can be useful in EMI shielding material.

Acknowledgments We are very thankful for the financial aid to this work provided by the Jaypee University of Information Technology, Waknaghat, Solan, Himachal Pradesh, India.

References

1. Suzuki, T., Tanaka, T., Ikemizu, K.: High density recording capability for advanced particulate media. J. Magn. Magn. Mater. **235**, 159 (2001)
2. Olsen, E., Thonstad, J.: Nickel ferrite as inert anodes in aluminium electrolysis. J. Appl. Electrochem. **29**, 293 (1999)
3. Gubbala, S., Nathani, H., Koizol, K., Misra, R.D.K.: Magnetic properties of nanocrystalline Zn–Mn, and Ni–Mn ferrites synthesized by reverse micelle technique. Phys. B Condens. Matter **348**, 317 (2004)
4. Rao, B.P., Rao, K.H.: Initial permeability dependence on the microstructural and compositional changes in Ni-Zn-Sc ferrites Le. J. Phys. **7**, 239 (1997)
5. Costa, A.C.F.M., Tortella, E., Morelli, M.R., Kiminami, R.H.G.A.: Synthesis, microstructure and magnetic properties of Ni–Zn ferrites. J. Magn. Magn. Mater. **256**, 174 (2003)
6. Da Silva, J.B., Mohallem, N.D.S.: Preparation of composites of nickel ferrites dispersed in silica matrix. J. Magn. Magn. Mater. **226**, 1393 (2001)
7. Jalaly, M., Enayati, M.H., Karimzadeh, F.: Investigation of structural and magnetic properties of nanocrystalline $Ni_{0.3}Zn_{0.7}Fe_2O_4$ prepared by high energy ball milling. J. Alloys Compd. **480**, 737 (2009)

8. Sertkol, M., Köseoğlu, Y., Baykal, A., Kavas, H., Başaran, A.C.: Synthesis and magnetic characterization of $Zn_{0.6}Ni_{0.4}Fe_2O_4$ nanoparticles via a polyethylene glycol-assisted hydrothermal route. J. Magn. Magn. Mater. **321**, 157 (2009)
9. Shannigrahi, S.R., Pramoda, K.P., Nugroho, F.A.A.: Synthesis and characterizations of microwave sintered ferrite powders and their composite films for practical applications. J. Magn. Magn. Mater. **324**, 140 (2012)
10. Rezlescu, E., Sachelarie, L., Popa, P.D., Rezlescu, N.: Effect of substitution of divalent ions on the electrical and magnetic properties of Ni-Zn-Me ferrites. IEEE Trans. Magn. **36**, 3962 (2000)
11. Rao, B.P., Caltun, O.F.: Microstructure and magnetic behaviour of Ni-Zn-Co ferrites. J. Optoelectron. Adv. Mater. **8**, 995 (2006)
12. Shannigrahi, S.R., Pramoda, K.P., Nugroho, F.A.A.: Synthesis and characterizations of microwave sintered ferrite powders and their composite films for practical applications. J. Magn. Magn. Mater. **324**, 140 (2012)
13. Shen, X., Wang, Y., Yang, X., Xia, Y., Zhuang, J.F., Tang, P.D.: Megahertz magneto-dielectric properties of nanosized NiZnCo ferrite from CTAB-assisted hydrothermal process . Trans. Nonferrous Metals Soc. China **19**, 1588 (2009)
14. Ghodake, J.S., Kambale, R.C., Kulkarni, S.D., Sawant, S.R., Suryavanshi, S.S.: Complex permeability studies of Ni–Co–Zn ferrites synthesized by an oxalate precursor method. Smart Mater. Struct. **18**, 125009 (2009)
15. Pereira, S.L., Pfannes, H.-D., Mendes Filho, A.A., Pinto, L.C.B., Chíncaro, M.A.: A comparative study of NiZn ferrites modified by the addition of cobalt. Mater. Res. **2**, 231 (1999)
16. Li, L.-Z., Peng, L., Zhu, X.-H., Yang, D.-Y.: Effects of cu and co substitution on the properties of Ni-Zn ferrite thin films. Journal of Electronic Science and Technology **10**, 88 (2012)
17. Yoo, B.S., Chae, Y.G., Kwon, Y.M., Kim, D.H., Lee, B.W., Liu, C.: Effects of solution concentration on the structural and magnetic properties of $Ni_{0.5}Zn_{0.5}Fe_2O_4$ ferrite nanoparticles prepared by sol-gel. J. Magn. **18**, 230 (2013)
18. Kwon, Y.M., Lee, M.Y., Mustaqima, M., Liu, C., Lee, B.W.: Structural and magnetic properties of $Ni_{0.6}Zn_{0.4}Fe_2O_4$ ferrite prepared by solid state reaction and sol-gel. J. Magn. **19**, 64 (2014)
19. George, M., Nair, S.S., John, A.M., Joy, P.A., Anantharaman, M.R.: Structural magnetic and electrical properties of the sol-gel prepared $Li_{0.5}Fe_{2.5}O_4$ fine particles. J. Phys. D. Appl. Phys. **39**, 900 (2006)
20. Prabahar, S., Dhanam, M.: CdS thin films from two different chemical baths—structural and optical analysis. J. Cryst. Growth **285**, 41 (2005)
21. Iqbal, M.J., Siddiquah, M.R.: Structural, electrical and magnetic properties of Zr–Mg cobalt ferrite. J. Magn. Magn. Mater. **320**, 845 (2008)
22. Ahlawat, A., Sathe, V.G., Reddy, V.R., Gupta, A.: Mossbauer Ramaand X-ray diffraction studies of superparamagnetic $NiFe_2O_4$ nanoparticles prepared by sol–gel auto-combustion method. J. Magn. Magn. Mater. **323**, 2049 (2011)
23. Neel, L.: Théorie du trâınagemagnétique des ferromagnétiques en grains fins avec applications auxterres cuites. Ann. Geophys. **5**, 99 (1949)
24. Bercoff, P.G., Bertorello, H.R.: Localized canting effect in Zn-substituted Ni ferrites. J. Magn. Magn. Mater. **213**, 56 (2000)
25. Shen, X., Wang, Y., Yang, X., Lu, L., Huang, L.: 0.3–3 GHz magneto-dielectric properties of nanostructured NiZnCo ferrite from hydrothermal process. J. Mater. Sci: Mater. Electron. **2**, 630 (2010)
26. Thakur, S., Katyal, S.C., Singh, M.: Structural and magnetic properties of nano nickel–zinc ferrite synthesized by reverse micelle technique. J. Magn. Magn. Mater. **321**, 1 (2009)